

Interaction-based quantum metrology showing scaling beyond the Heisenberg limit.

M. Napolitano¹, M. Koschorreck¹, B. Dubost^{1,2}, N. Behbood¹, R. J. Sewell¹ & M. W. Mitchell¹

¹*ICFO-Institut de Ciències Fòniques, Mediterranean Technology Park, 08860 Castelldefels (Barcelona), Spain.*

²*Laboratoire Matériaux et Phénomènes Quantiques, Université Paris Diderot et CNRS, UMR 7162, Bât. Condorcet, 75205 Paris Cedex 13, France.*

Quantum metrology studies the use of entanglement and other quantum resources to improve precision measurement¹. An interferometer using N independent particles to measure a parameter \mathcal{X} can achieve at best the “standard quantum limit” (SQL) of sensitivity $\delta\mathcal{X} \propto N^{-1/2}$. The same interferometer² using N entangled particles can achieve in principle the “Heisenberg limit” $\delta\mathcal{X} \propto N^{-1}$, using exotic states³. Recent theoretical work argues that *interactions* among particles may be a valuable resource for quantum metrology, allowing scaling beyond the Heisenberg limit⁴⁻⁶. Specifically, a k -particle interaction will produce sensitivity $\delta\mathcal{X} \propto N^{-k}$ with appropriate entangled states and $\delta\mathcal{X} \propto N^{-(k-1/2)}$ even without entanglement⁷. Here we demonstrate this “super-Heisenberg” scaling in a nonlinear, non-destructive^{8,9} measurement of the magnetisation^{10,11} of an atomic ensemble¹². We use fast optical nonlinearities to generate a pairwise photon-photon interaction¹³ ($k = 2$) while preserving quantum-noise-limited performance^{7,14}, to produce $\delta\mathcal{X} \propto N^{-3/2}$. We observe super-Heisenberg scaling over two orders of magnitude in N , limited at large N by higher-order

nonlinear effects, in good agreement with theory¹³. For a measurement of limited duration, super-Heisenberg scaling allows the nonlinear measurement to overtake in sensitivity a comparable linear measurement with the same number of photons. In other scenarios, however, higher-order nonlinearities prevent this crossover from occurring, reflecting the subtle relationship of scaling to sensitivity in nonlinear systems. This work shows that inter-particle interactions can improve sensitivity in a quantum-limited measurement, and introduces a fundamentally new resource for quantum metrology.

The best instruments are interferometric in nature, and operate according to the laws of quantum mechanics. A collection of particles, e.g., photons or atoms, is prepared in a superposition state, allowed to evolve under the action of a Hamiltonian containing an unknown parameter \mathcal{X} , and measured in agreement with quantum measurement theory. The complementarity of quantum measurements¹⁵ determines the ultimate sensitivity of these instruments.

Here we describe polarisation interferometry, used for example in optical magnetometry to detect atomic magnetisation^{11,16,17}; similar theory describes other interferometers². A collection of N photons, with circular plus/minus polarisations $|+\rangle, |-\rangle$ is described by single-photon Stokes operators $\hat{s}_i = \frac{1}{2}(|+\rangle, |-\rangle)\sigma_i(\langle+|, \langle-|)^T$, where the σ_i are the Pauli matrices and σ_0 is the identity. In traditional quantum metrology, a Hamiltonian of the form $\hat{H} = \hbar\mathcal{X} \sum_{j=1}^N \hat{s}_z^{(j)}$ uniformly and independently couples the photons to \mathcal{X} , the parameter to be measured¹. If the input state consists of independent photons, the possible precision scales as $\delta\mathcal{X} \propto N^{-1/2}$, the shot-noise or standard quantum limit (SQL). The $N^{-1/2}$ factor reflects the statistical averaging of independent results.

In contrast, entangled states can be highly, even perfectly, correlated, giving precision limited by $\delta\mathcal{X} \propto N^{-1}$, the Heisenberg limit (HL).

The above Hamiltonian is conveniently written $\hat{H} = \hbar\mathcal{X}\hat{S}_z$, where $\hat{S}_i \equiv \sum_{j=1}^N \hat{s}_i^{(j)}$ is a collective variable describing the net polarisation of the photons. The independence of the photons manifests itself in the linearity of this Hamiltonian. Recently Boixo *et al.* have shown that interactions among particles, or equivalently nonlinear Hamiltonians, can contribute to measurement sensitivity and give scaling beyond the Heisenberg limit⁴. For example, a Hamiltonian $\hat{H} = \hbar\mathcal{X}\hat{S}_z^k$, i.e., with a k -order nonlinearity in \hat{S} , contains k -photon interaction terms $\hat{s}_z^{(j_1)} \otimes \hat{s}_z^{(j_2)} \otimes \dots \otimes \hat{s}_z^{(j_k)}$. The number of such terms, and thus the signal strength, grows as N^k , while the quantum noise from the input states is unchanged. As a result, a sensitivity limit of $\delta\mathcal{X} \propto N^{-k}$ applies when entanglement is used, and $\delta\mathcal{X} \propto N^{-(k-1/2)}$ in the absence of entanglement⁷. For $k \geq 2$, this already gives a scaling better than the Heisenberg limit, so-called “super-Heisenberg” (SH) scaling⁷. Note that interactions and entanglement are compatible and both improve the scaling. The predicted advantage applies generally to quantum interferometry, and proposed mechanisms to produce metrologically-relevant interactions include Kerr nonlinearities¹⁸, cold collisions in condensed atomic gases⁷, Duffing nonlinearity in nano-mechanical resonators¹⁹ and a two-pass effective nonlinearity with an atomic ensemble²⁰. Topological excitations in nonlinear systems may also give advantageous scaling²¹.

In this Letter, we study interaction-based quantum metrology using unentangled probe particles. One challenge in demonstrating SH scaling is to engineer a suitable nonlinear Hamiltonian.

Some nonlinearities have been shown to be intrinsically noisy¹⁴ while others give SH scaling but fall short of the ideal $N^{-(k-1/2)}$ under realistic conditions^{7,22}. We use a cold atomic ensemble as a light-matter quantum interface¹² to produce quantum-noise-limited interactions and a Hamiltonian of the form $\hat{H} = \hbar\mathcal{X}\hat{S}_z\hat{S}_0 = \hbar\mathcal{X}\hat{S}_zN/2$. This Hamiltonian gives a polarisation rotation growing with the photon number, without increasing quantum noise⁷. The experiment, shown schematically in Fig. 1, uses pulses of near-resonant light to measure the collective spin $\hat{\mathbf{F}}$ of an ensemble of $N_A \sim 10^6$ cold rubidium-87 atoms, probed on the $5S_{1/2} \rightarrow 5P_{3/2}$ D₂ line. The experimental system is described in detail in the references^{8,23}. The on-axis atomic magnetisation $\langle \hat{F}_z \rangle$, which plays the role of \mathcal{X} in this measurement, is prepared in the initial state $\langle \hat{F}_z \rangle = N_A$ by optical pumping with resonant circularly polarised light propagating along the trap axis z . A weak on-axis magnetic field is applied to preserve \hat{F}_z during the measurements.

Pulses of \hat{S}_x polarised, but not entangled, photons pass through the ensemble and experience an optical rotation proportional to $\langle \hat{F}_z \rangle$. The light-atom interaction Hamiltonian $\hat{H}_{\text{eff}} = \alpha^{(1)}\hat{F}_z\hat{S}_z + \beta^{(1)}\hat{F}_z\hat{S}_zN/2$ describes this paramagnetic Faraday rotation¹³. Both the linear term $\alpha^{(1)}\hat{F}_z\hat{S}_z$ and the nonlinear term $\beta^{(1)}\hat{F}_z\hat{S}_zN/2$ cause rotation of the plane of polarisation from \hat{S}_x (vertical) toward \hat{S}_y (diagonal). Detection of \hat{S}_y then allows estimation of \hat{F}_z . As described in the Supplementary Information, $\alpha^{(1)}$ and $\beta^{(1)}$ depend on the optical detuning Δ relative to the $F = 1 \rightarrow F' = 0$ transition, in particular $\alpha^{(1)}(\Delta_0) = 0$ for the specific detuning $\Delta_0 \approx 2\pi(468.5 \text{ MHz})$, allowing a purely nonlinear estimation to be studied.

The rotation angle is $\phi = \langle \hat{F}_z \rangle [A(\Delta) + B(\Delta)N]/2$ where $A \propto \alpha^{(1)}$ and $B \propto \beta^{(1)}$ account

for the temporal pulse shape and geometric overlap between the atomic density and the spatial mode of the probe. The shot-noise limited uncertainty in the rotation angle, due to quantum uncertainty in the initial angle, is $\delta\phi = N^{-1/2}/2$. A contribution $\langle \hat{F}_z \rangle B(\Delta)\delta N/2$ from initial number fluctuations $\delta N = \langle N \rangle^{-1/2}$ is negligible for small rotation angles. This gives a measurement uncertainty

$$\delta F_z = \langle \hat{F}_z \rangle \frac{\delta\phi}{\phi} = \frac{1}{A(\Delta)N^{1/2} + B(\Delta)N^{3/2}}, \quad (1)$$

indicating a transition from SQL scaling $\delta F_z \propto N^{-1/2}$ to SH scaling $\delta F_z \propto N^{-3/2}$ with increasing N .

Two regimes of probing are used: the *linear probe* consists of forty $1\ \mu\text{s}$ pulses (total illumination time $\tau_L = 40\ \mu\text{s}$) spread over $400\ \mu\text{s}$ with detuning $\Delta_L \gg \Delta_0$. This gives $A \gg N_L B$, i.e., linear estimation and, as described by Koschorreck *et al.*⁸, provides a projection-noise-limited quantum-non-demolition (QND) measurement²⁴ of \hat{F}_z , with uncertainty at the parts-per-thousand level⁸. The *nonlinear probe* consists of a single $\tau_{NL} = 54\ \text{ns}$ FWHM, Gaussian-shaped, high-intensity pulse with N_{NL} photons and detuning Δ_0 , so that $A \ll N_{NL} B$. Crucially, having two probes allows us to precisely calibrate the nonlinear measurement using a highly sensitive and well characterised independent measurement of the same sample.

We probe the same sample three times for each preparation: First with the linear probe, which gives a precise and non-destructive measurement of $\langle \hat{F}_z \rangle$ via a rotation ϕ_L . Then with the nonlinear probe, contributing with a rotation ϕ_{NL} , which is calibrated against the “true” value (i.e., with negligible error) provided by the previous linear probe. Third, a second linear probe is used

to estimate the damage to the atomic magnetisation $\eta \equiv 1 - \phi_{L'}/\phi_L$ caused by the nonlinear probe.

The linear probe is calibrated using quantitative absorption imaging to measure N_A , and we find $A(\Delta_L) = 3.3(1) \times 10^{-8}$ rad per atom. The calibration of the nonlinear probe against the first linear probe is shown in Fig. 2: We repeat the above pump/probe sequence while varying N_A in the range $N_A = 1.5 \times 10^5$ to $N_A = 3.5 \times 10^5$ to generate a ϕ_L, ϕ_{NL} correlation plot for a given N_{NL} . Since both ϕ_L and ϕ_{NL} are linear in N_A , we use linear regression to find the slope $b = d\phi_{NL}/d\phi_L = B(\Delta_0)N_{NL}/A(\Delta_L)$ for that value of N_{NL} . The experiment is repeated varying the number of photons N_{NL} in the nonlinear pulse.

The observed b vs. N_{NL} , shown in Fig. 2a, is well fit by a simple model including saturation of the nonlinear response:

$$\frac{d\phi_{NL}}{d\phi_L} = \frac{B(\Delta_0)N_{NL}}{A(\Delta_L)} \frac{1}{1 + N_{NL}/N_{NL}^{(\text{sat})}}, \quad (2)$$

with a saturation parameter $N_{NL}^{(\text{sat})} = 6.0(8) \times 10^7$ and the nonlinear coupling strength $B(\Delta_0) = 3.8(2) \times 10^{-16}$ rad per atom per photon.

The noise in the nonlinear probe, again as a function of N_{NL} , is determined from the ϕ_L, ϕ_{NL} correlation plots. As illustrated in Fig. 2b-c, the residual standard deviation of the fits indicates the observed uncertainty $\Delta\phi_{NL}$, which includes the intrinsic uncertainty $\delta\phi_{NL}$ and a small contribution from electronic noise. In Fig. 3 we plot the fractional sensitivity $\delta F_z^{(\text{NL})} / \langle \hat{F}_z \rangle$ vs. N_{NL} , calculated

using equation (2) and considering the whole polarised ensemble, $\langle \hat{F}_z \rangle = 7 \times 10^5$. In agreement with equation (1), the log-log slope indicates the scaling $\delta F_z^{(\text{NL})} \propto N_{\text{NL}}^{-3/2}$ to within experimental uncertainties in the range $N_{\text{NL}} = 10^6$ to $N_{\text{NL}} = 10^7$, and SH scaling, i.e., steeper than N^{-1} , over two orders of magnitude $N_{\text{NL}} = 5 \times 10^5$ to $N_{\text{NL}} = 5 \times 10^7$.

Results of numerical modelling using the Maxwell-Bloch equations to describe the non-linear light-atom interaction are also shown in Fig. 3. Two curves are shown, for detunings $\Delta_0 \pm 2\pi(200 \text{ kHz})$, covering the combined uncertainty in Δ due to the probe laser linewidth and inhomogeneous light shifts in the optical dipole trap. As expected from equation (1), this alters the sensitivity only at low N_{NL} . The model is described in detail in the Supplementary Information.

For photon numbers above $N_{\text{NL}} \gtrsim 2 \times 10^7$, the saturation of the nonlinear rotation alters the slope. This can be understood as optical pumping of atoms into states other than $|F = 1, m_F = 1\rangle$ by the nonlinear probe. The damage to the atomic magnetisation $\eta = 1 - \phi_{L'}/\phi_L$, shown in Fig. 3 remains small, confirming the non-destructive nature of the measurement. The finite damage even for small N_{NL} is possibly due to stray light and/or magnetic fields disturbing the atoms during the 20 ms period between the two linear measurements. At large N , high-order nonlinear effects including optical pumping limit the range of SH scaling.

The experimental results illustrate the subtle relationship of scaling to sensitivity in a non-linear system. For an ideal nonlinear measurement, the improved scaling would guarantee better absolute sensitivity for sufficiently large N . Indeed, when the measurement bandwidth is taken into account, the nonlinear probe overtakes the linear one at $N = 3.2 \times 10^6$ where both achieve a

sensitivity of 1.1×10^2 spins $\text{Hz}^{-1/2}$. As a consequence, the nonlinear technique performs better in fast measurements. In contrast, when measurement time is not a limited resource, the comparison can be made on a “sensitivity-per-measurement” basis, and the ideal crossover point of 3.2×10^3 spins at $N = 8.7 \times 10^7$ is never actually reached, due to the higher-order nonlinearities. Evidently SH scaling enables but does not guarantee enhanced sensitivity: for the nonlinear to overtake the linear, it is also necessary that the scaling extend to large enough N . The comparison shows also that resource constraints dramatically influence the linear vs. nonlinear comparison. See also the Supplementary Information.

We have realised a scenario proposed by Boixo *et al.*⁴ to achieve metrological sensitivity beyond the Heisenberg limit $\delta\mathcal{X} \propto N^{-1}$ using metrologically-relevant interactions among particles. To generate pairwise photon-photon interactions, we use fast nonlinear optical effects in a cold atomic ensemble and measure the ensemble magnetisation $\langle \hat{F}_z \rangle$ with super-Heisenberg sensitivity $\delta F_z \propto N^{-3/2}$. To rigorously quantify the photon-photon interaction and the sensitivity, we calibrate against a precise, non-destructive, linear measurement of the same atomic quantity⁸, demonstrate quantum-noise-limited performance of the optical instrumentation, and place an upper limit on systematic, i.e., non-atomic, nonlinearities at the few-percent level. The experiment demonstrates the use of inter-particle interactions as a new resource for quantum metrology. While possible applications to precision measurement will require detailed study, this first experiment shows that interactions can produce super-Heisenberg scaling and improved precision in a quantum-limited measurement.

Methods

Linear & nonlinear probe light. The probe beam is aligned to the axis of the trap with a waist of $20\ \mu\text{m}$, chosen to match the radial dimension of the cloud. In the linear probing regime we use a train of forty $1\ \mu\text{s}$ pulses, pulse period $10\ \mu\text{s}$, each containing 3×10^6 photons detuned $+1.5\ \text{GHz}$ from the ($F = 1 \rightarrow F' = 0$) transition. The maximum intensity is $0.1\ \text{Wcm}^{-2}$. The signals are summed and can be considered a single, modulated pulse.

The nonlinear probe consists of a single Gaussian-shaped pulse with a FWHM of $54\ \text{ns}$. The maximum intensity of the nonlinear probe is $7\ \text{Wcm}^{-2}$ for a pulse with 10^7 photons. Theory predicts $\alpha^{(1)} = 0$ at a detuning $\Delta = 2\pi(462\ \text{MHz})$ in free space. This is modified by trap-induced light shifts, and we use the empirical value $\Delta_0 = 2\pi(468.5\ \text{MHz})$, which gives zero rotation at low probe intensity.

Instrumental noise. The instrumental noise is quantified by measuring $\text{var}(\hat{S}_y)$ vs. input photon number N ($= N_L$ or N_{NL}), in the absence of atoms, to find contributions from electronic noise $V^{(\text{el})} \propto N^0$, shot-noise $= N^1$, and technical noise $\propto N^2$, as described in the Supplementary Information. We find $V_L^{(\text{el})}$ and $V_{\text{NL}}^{(\text{el})}$ are 3×10^5 and 4×10^5 per pulse, respectively, while the technical noise is negligible. The instrumentation is thus shot-noise-limited over the full range of N used in the experiment. The intrinsic rotation uncertainty of the nonlinear probe $\delta\phi_{\text{NL}}$ is calculated from the measured $\Delta\phi_{\text{NL}}$ as $(\delta\phi_{\text{NL}})^2 = (\Delta\phi_{\text{NL}})^2 - V_{\text{NL}}^{(\text{el})}$. The correction is at most 5%.

Instrumental linearity. The linearity of the experimental system and analysis is verified using a wave-plate in place of the atoms to produce a linear rotation equal to the largest observed nonlinear

rotation. Over the full range of photon numbers used in the experiment, the detected rotation angle is constant to within 5%, and SQL scaling is observed.

1. Giovannetti, V., Lloyd, S. & Maccone, L. Quantum metrology. *Phys. Rev. Lett.* **96**, 010401 (2006).
2. Lee, H., Kok, P. & Dowling, J. P. A quantum Rosetta stone for interferometry. *J. Mod. Opt.* **49**, 2325–2338 (2002).
3. Mitchell, M. W., Lundeen, J. S. & Steinberg, A. M. Super-resolving phase measurements with a multiphoton entangled state. *Nature* **429**, 161–164 (2004).
4. Boixo, S., Flammia, S. T., Caves, C. M. & Geremia, J. Generalized limits for single-parameter quantum estimation. *Phys. Rev. Lett.* **98**, 090401 (2007).
5. Choi, S. & Sundaram, B. Bose-Einstein condensate as a nonlinear Ramsey interferometer operating beyond the Heisenberg limit. *Phys. Rev. A* **77**, 053613 (2008).
6. Roy, S. M. & Braunstein, S. L. Exponentially enhanced quantum metrology. *Phys. Rev. Lett.* **100**, 220501 (2008).
7. Boixo, S. *et al.* Quantum metrology: Dynamics versus entanglement. *Phys. Rev. Lett.* **101**, 040403 (2008).
8. Koschorreck, M., Napolitano, M., Dubost, B. & Mitchell, M. W. Sub-projection-noise sensitivity in broadband atomic magnetometry. *Phys. Rev. Lett.* **104**, 093602 (2010).

9. Koschorreck, M., Napolitano, M., Dubost, B. & Mitchell, M. W. Quantum nondemolition measurement of large-spin ensembles by dynamical decoupling. *Phys. Rev. Lett.* **105**, 093602 (2010).
10. Kominis, I., Kornack, T., Allred, J. & Romalis, M. A subfemtotesla multichannel atomic magnetometer. *Nature* **422**, 596–599 (2003).
11. Budker, D. & Romalis, M. Optical magnetometry. *Nature Phys.* **3**, 227 – 234 (2007).
12. Hammerer, K., Sørensen, A. S. & Polzik, E. S. Quantum interface between light and atomic ensembles. *Rev. Mod. Phys.* **82**, 1041–1093 (2010).
13. Napolitano, M. & Mitchell, M. W. Nonlinear metrology with a quantum interface. *New J. Phys.* **12**, 093016 (2010).
14. Fleischhauer, M., Matsko, A. B. & Scully, M. O. Quantum limit of optical magnetometry in the presence of ac stark shifts. *Phys. Rev. A* **62**, 013808 (2000).
15. Scully, M. O., Englert, B. G. & Walther, H. Quantum optical tests of complementarity. *Nature* **351**, 111–116 (1991).
16. Wasilewski, W. *et al.* Quantum noise limited and entanglement-assisted magnetometry. *Phys. Rev. Lett.* **104**, 133601 (2010).
17. Wolfgramm, F. *et al.* Squeezed-light optical magnetometry. *Phys. Rev. Lett.* **105**, 053601 (2010).

18. Beltrán, J. & Luis, A. Breaking the Heisenberg limit with inefficient detectors. *Phys. Rev. A* **72**, 045801 (2005).
19. Woolley, M. J., Milburn, G. J. & Caves, C. M. Nonlinear quantum metrology using coupled nanomechanical resonators. *New J. Phys.* **10**, 125018 (2008).
20. Chase, B. A., Baragiola, B. Q., Partner, H. L., Black, B. D. & Geremia, J. M. Magnetometry via a double-pass continuous quantum measurement of atomic spin. *Phys. Rev. A* **79**, 062107 (2009).
21. Negretti, A., Henkel, C. & Molmer, K. Quantum-limited position measurements of a dark matter-wave soliton. *Phys. Rev. A* **77**, 043606 (2008).
22. Boixo, S. *et al.* Quantum-limited metrology and Bose-Einstein condensates. *Phys. Rev. A* **80**, 032103 (2009).
23. Kubasik, M. *et al.* Polarization-based light-atom quantum interface with an all-optical trap. *Phys. Rev. A* **79**, 043815 (2009).
24. Braginskii, V. B. & Vorontsov, Y. I. Quantum-mechanical limitations in macroscopic experiments and modern experimental technique. *Sov. Phys. Usp.* **17**, 644 (1975).

Acknowledgements We thank I. H. Deutsch and F. Illuminati, for helpful comments. We thank C. M. Caves and A. D. Codorniu for inspiration. This work was supported by the Spanish Ministry of Science and Innovation through the Consolider-Ingenio 2010 project QOIT, Ingenio-Explora project OCHO (Ref. FIS2009-07676-E/FIS), project ILUMA (Ref. FIS2008-01051) and by the Marie-Curie RTN EMALI.

Author Contributions All authors contributed equally to the work presented in this paper.

Competing Interests The authors declare that they have no competing financial interests.

Correspondence Correspondence and requests for materials should be addressed to Mario Napolitano (email: mario.napolitano@icfo.es).

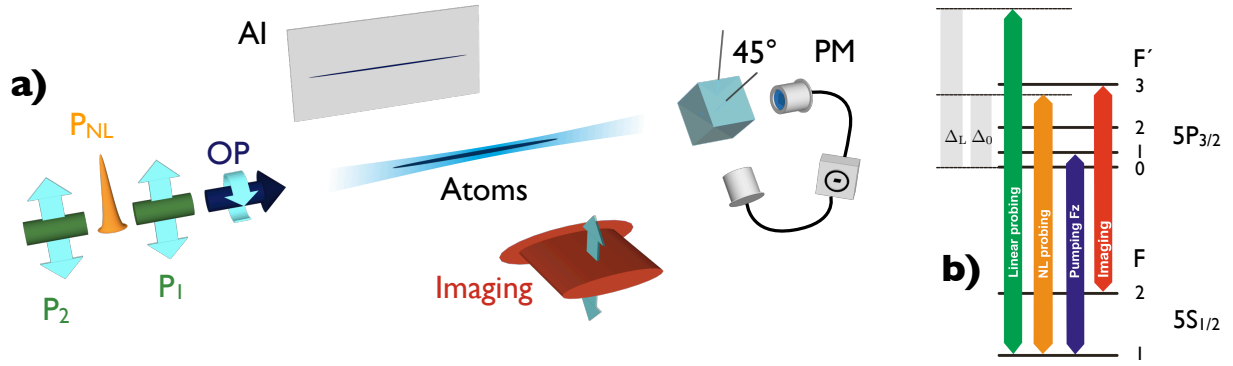


Figure 1: **Atom-light interface** a) Experimental schematic: an ensemble of 7×10^5 ^{87}Rb atoms, held in an optical dipole trap, is prepared in $|F = 1, m_F = 1\rangle$ by optical pumping (OP). Linear (P_1), nonlinear (P_{NL}), and a second linear (P_2) Faraday rotation probe pulses measure the atomic magnetisation, detected by a shot-noise-limited polarimeter (PM). The atom number is measured by quantitative absorption imaging (AI). b) Spectral positions of the pumping, probing, and imaging light on the D_2 transition.

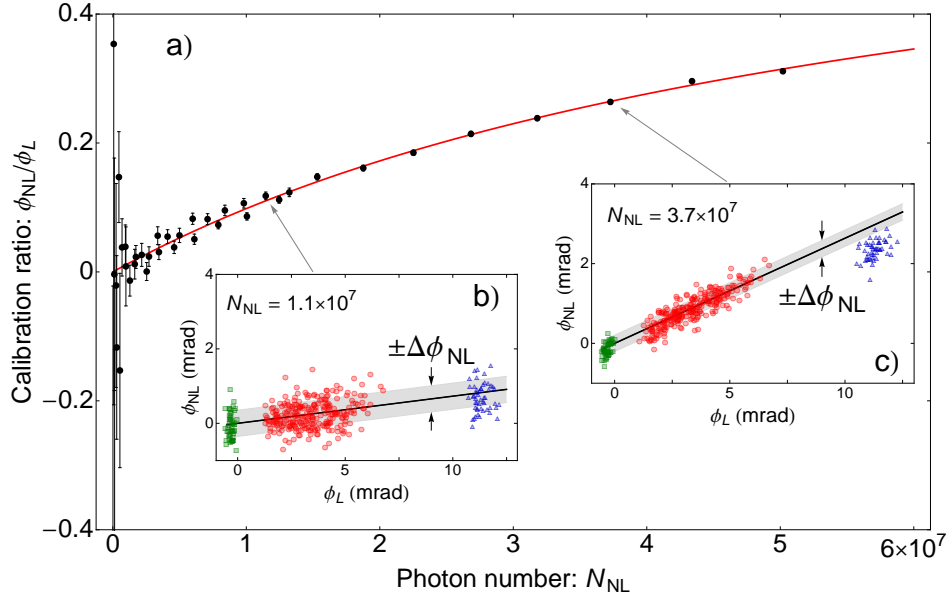


Figure 2: **Calibration of nonlinear Faraday rotation.** a) Ratio of nonlinear rotation ϕ_{NL} to linear rotation ϕ_L vs. nonlinear probe photon number N_{NL} . The data points and error bars indicate best fit and standard errors from a linear regression $\phi_{NL} = b\phi_L + \text{const.}$ for a given N_{NL} . The red curve is a fit with equation (2), showing the expected nonlinear behaviour $\phi_{NL} \propto N_{NL}$, with some saturation for large N_{NL} . b) & c) ϕ_L, ϕ_{NL} correlation plots for two values of N_{NL} . The atom number N_A is varied to produce a range of ϕ_L and ϕ_{NL} . Green squares: no atoms $N_A = 0$, red circles: $1.5 \times 10^5 < N_A < 3.5 \times 10^5$, blue triangles $N_A \approx 7 \times 10^5$. The blue triangles are shown as a check on detector saturation, and are not included in the analysis.

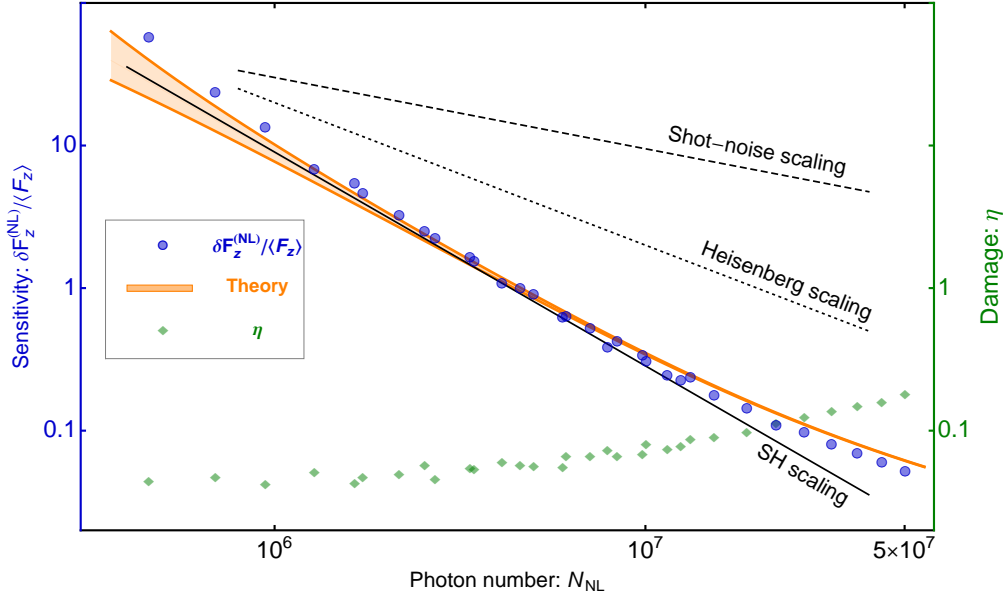


Figure 3: **Super-Heisenberg scaling.** Fractional sensitivity $\delta F_z^{(NL)} / \langle \hat{F}_z \rangle$ of the nonlinear probe versus number of interacting photons N_{NL} . Blue circles indicate the measured sensitivity, curves show results of numerical modelling, and the black lines indicate SQL, HL, and SH scaling for reference. Scaling surpassing the Heisenberg limit $\propto N_{NL}^{-1}$ is observed over two orders of magnitude. The measured damage η to the magnetisation, shown as green diamonds, confirms the non-destructive nature of the measurement. Error bars for standard errors would be smaller than the symbols and are not shown.

Supplementary Information for “Interaction-based quantum metrology showing scaling beyond the Heisenberg limit.”

M. Napolitano¹, M. Koschorreck¹, B. Dubost^{1,2}, N. Behbood¹, R. J. Sewell¹ & M. W. Mitchell¹

¹*ICFO-Institut de Ciències Fotoniques, 08860 Castelldefels (Barcelona), Spain.*

²*Laboratoire Matériaux et Phénomènes Quantiques, Université Paris Diderot et CNRS, UMR 7162, Bât. Condorcet, 75205 Paris Cedex 13, France.*

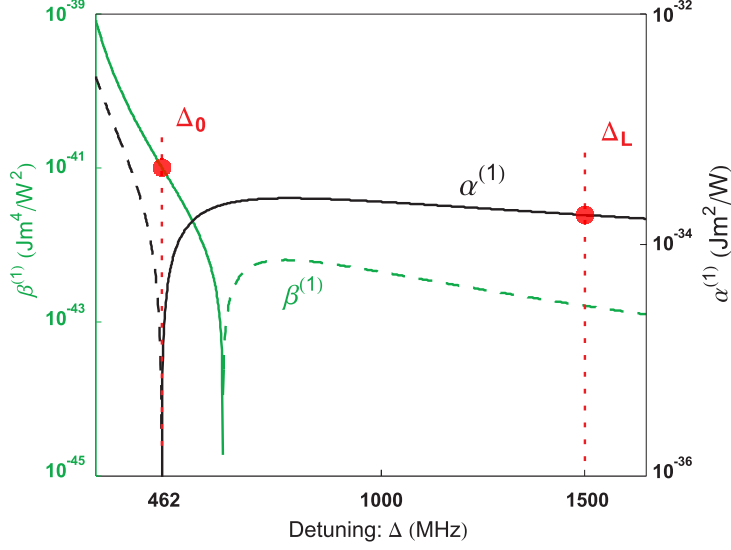
1 Supplementary Discussion

Interaction Hamiltonian. The atom-light interaction is described using collective continuous variables and degenerate perturbation theory in reference [13] of the main text. We repeat essential results:

The electric dipole interaction $h_{\text{int}} = -\mathbf{E} \cdot \mathbf{d}$, taken in second order perturbation theory, gives rise to an effective (single-atom) Hamiltonian of the form

$$H_{\text{eff}}^{(2)} = \alpha^{(1)} \hat{S}_z \hat{J}_z + \alpha^{(2)} \left(\hat{S}_x \hat{J}_x + \hat{S}_y \hat{J}_y \right), \quad (\text{S1})$$

plus terms in \hat{S}_0 which do not alter the optical polarisation. Here $\alpha^{(1)}, \alpha^{(2)}$ describe the vectorial and tensorial components of the interaction respectively, and the atomic collective variable is $\hat{\mathbf{J}} \equiv \sum_i \hat{\mathbf{j}}^{(i)}$ where the superscript (i) indicates the i 'th atom and $\hat{j}_x \equiv (\hat{f}_x^2 - \hat{f}_y^2)/2$,



Supp. Fig. 1: Spectra of the terms of the effective Hamiltonian. Black curve and right axis correspond to $\alpha^{(1)}$; Green curve and left axis to $\beta^{(1)}$. The curves are dashed when the coefficient assumes negative value. Detuning [MHz] is relative to the $F = 1 \rightarrow F' = 0$ of ^{87}Rb D_2 transition. The detunings of the two probing regimes used in the experiment are indicated.

$\hat{j}_y \equiv (\hat{f}_x \hat{f}_y + \hat{f}_y \hat{f}_x)/2$, $\hat{j}_z \equiv \hat{f}_z/2$ and $\hat{j}_0 \equiv \hat{f}_z^2/2$. For our case of the $F=1$ ground state, the $\hat{\mathbf{j}}$ operators, defined starting from the angular momentum operators $\hat{\mathbf{f}}$, represent a pseudo-spin 1/2 system involving the states $m_f = \pm 1$. In this representation, the measurement of \hat{F}_z , described in the main text, is equally to a measurement of $2\hat{J}_z = \hat{F}_z$.

For $F = 1$ atoms, the fourth-order contribution (again ignoring terms depending only on \hat{S}_0) is:

$$H_{\text{eff}}^{(4)} = \beta_J^{(0)} \hat{S}_z^2 \hat{J}_0 + \beta_N^{(0)} \hat{S}_z^2 N_A + \beta^{(1)} \hat{S}_0 \hat{S}_z \hat{J}_z + \beta^{(2)} \hat{S}_0 (\hat{S}_x \hat{J}_x + \hat{S}_y \hat{J}_y). \quad (\text{S2})$$

For our input state, consisting of N vertically-polarized photons, i.e., $\langle (\hat{S}_x, \hat{S}_y, \hat{S}_z) \rangle = (N/2, 0, 0)$, we can drop all but the $\alpha^{(1)}$ and $\beta^{(1)}$ terms, because 1) terms in \hat{S}_x and $\hat{S}_0 \hat{S}_x$, leave the initial state unchanged, 2) terms in \hat{S}_y and $\hat{S}_0 \hat{S}_y$ commute with the measured variable, giving no measurable signal and 3) the terms in \hat{S}_z^2 make a contributions smaller than the $\beta^{(1)}$ term by a factor $\sim \hat{S}_z/\hat{S}_0$.

The coefficients $\alpha^{(1)}$ and $\beta^{(1)}$ depend strongly on the probe frequency due to the excited

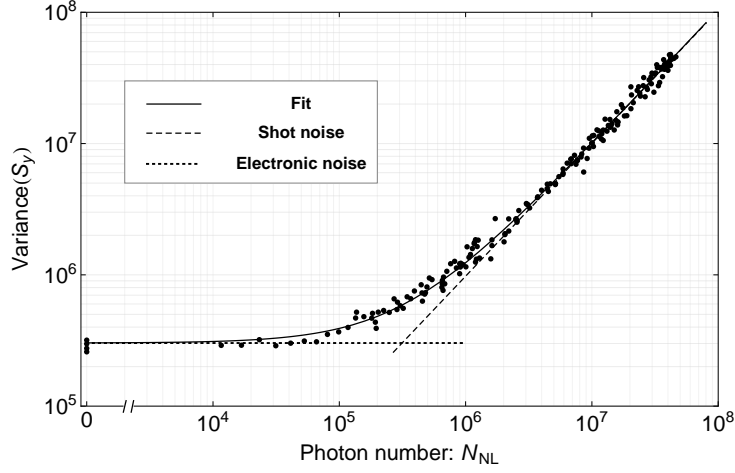
state hyperfine structure. For the D_2 line of ^{87}Rb , from the $F = 1$ ground state, they are shown graphically in Supp. Fig. 1.

We note also that $H_{\text{eff}}^{(4)}$ is sensitive to more spin degrees of freedom than is $H_{\text{eff}}^{(2)}$. The population of the state $|F = 1, m = 0\rangle$, i.e., $N_A - J_0$, appears in $H_{\text{eff}}^{(4)}$ proportional to \hat{S}_z^2 and produces polarization self-rotation. In contrast, $H_{\text{eff}}^{(2)}$ has no dependence on this population, which cannot be detected by any linear measurement.

Atomic State Preparation. The atomic ensemble contains up to 7×10^5 ^{87}Rb atoms held in an optical dipole trap formed by a weakly-focused ($52 \mu\text{m}$) beam of a Yb:YAG laser at 1030 nm with 6 W of optical power. The trap is loaded from a conventional magneto-optical trap (MOT) and cooled to 25 μK with sub-Doppler cooling. The system has demonstrated high effective optical depth²³ ($d_0 > 50$) and sub-projection-noise sensitivity⁸ of ~ 500 spins with the linear probe.

The ensemble is polarised $\langle \hat{F}_z \rangle = N_A$ by optical pumping with circularly polarised light resonant with the $F = 1 \rightarrow F' = 1$ transition, sent along the longitudinal axis of the trap. Repump light resonant with $F = 2 \rightarrow F' = 2$ is simultaneously applied via the 6 directions of the MOT beams to prevent accumulation in the $F = 2$ hyperfine level. A small bias magnetic field of 100 mG is applied along the axis to preserve \hat{F}_z .

Before each polarisation step, the state of the ensemble is reset to a fully-mixed state by repeated pumping from $F = 1$ to $F = 2$ and back, using resonant lasers from the MOT beams as described in Koschorreck *et al.*⁸. During the reset process, about 10% of the atoms escape from



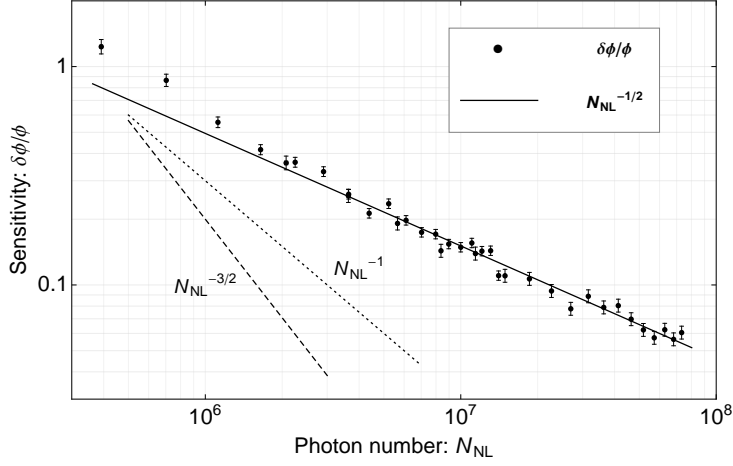
Supp. Fig. 2: Shot noise limited detection.

Detected variance in \hat{S}_y versus input photon number for short, intense pulses of the nonlinear probe. Points are measured variances, curve is a fit to $\text{var}(\hat{S}_y) = V_{\text{el}} + N_{\text{NL}}$, where V_{el} is the electronic noise. Negligible technical noise is seen. The system is shot-noise limited above $N_{\text{NL}} \gtrsim 4 \times 10^5$, i.e., for the full range used in the experiment.

the trap, allowing measurement with different N_A during a single loading cycle.

Shot noise limited detection. Before the ensemble, a beamsplitter and calibrated fast photodiode are used to detect the input pulse energy $\hat{S}_0 = \hat{S}_x$. After the ensemble, pulses are analyzed in the $\pm 45^\circ$ basis with an ultra-low-noise balanced photo-detector²⁵, giving a direct measure of \hat{S}_y . Both signals are recorded on a digital storage oscilloscope, and rotation angles calculated as $\phi = \hat{S}_y / (\hat{S}_x \sqrt{T_H T_V})$ where $T_{H,V}$ are the measured transmission coefficients for the system optics (vacuum cell, lenses and dichroic mirrors to separate the dipole trap beam). Supp. Fig. 2 shows the noise vs. power curve for generation and detection of nonlinear probe pulses, indicating an electronic noise contribution to $\text{var}(\hat{S}_y)$ of 4×10^5 per pulse. This electronic noise is subtracted when calculating $\delta\phi_{\text{NL}}$ in Fig. 3 of the main text.

System linearity. To check for systematic errors, both in the apparatus and in the analysis, we repeat the experiment under identical conditions but with no atoms present. We mimic the Faraday



Supp. Fig. 3: System linearity. Sensitivity results obtained as in Fig. 3 of the main text, but with a waveplate rotation in place of the atomic Faraday rotation. As expected the sensitivity shows SQL scaling, providing a direct verification of the linearity of the equipment and method of analysis. Error bars plotted are the standard errors of the measured rotation signal.

rotation signal by rotating the wave-plate used to balance the polarimeter to give a signal equal to the largest signal seen with atoms. The measured rotation is independent of N_{NL} , and gives shot-noise scaling of the sensitivity, plotted in Supp. Fig. (3) over the range of N_{NL} used in the experiment.

Modelling. We model the nonlinear rotation by integrating the Maxwell-Bloch equations in three spatial dimensions $\mathbf{x} = (x, y, z)$ plus time t . This semiclassical model describes the average rotation $\langle \phi \rangle = \langle \hat{S}_y^{(\text{out})} \rangle / \langle \hat{S}_x^{(\text{in})} \rangle$, which remains $\ll 1$, while the quantum noise is given by $\delta\phi = \delta\hat{S}_y^{(\text{out})} / \langle \hat{S}_x^{(\text{in})} \rangle \approx \delta\hat{S}_y^{(\text{in})} / N = 1/\sqrt{N}$.

In retarded coordinates $\zeta \equiv z$ and $\tau \equiv t - z/c$, the field envelope $\mathcal{E}(\mathbf{x}, \tau)$ and atomic state

$\rho(\mathbf{x}, \tau)$ obey the coupled equations

$$\mathcal{D}\mathcal{E} = \frac{k^2}{\varepsilon_0}\mathcal{P} \quad (\text{S3})$$

$$\partial_\tau\rho = \frac{i}{\hbar}[\rho, H(\mathcal{E})] + \mathcal{L}(\rho) \quad (\text{S4})$$

where $\mathcal{D} \equiv \partial_x^2 + \partial_y^2 + 2ik\partial_\zeta$ is the differential operator of the paraxial wave equation (PWE), k is the wave-number, \mathcal{L} is the Liouvillian describing relaxation and the polarization envelope $\mathcal{P}(\mathbf{x}, \tau)$ is

$$\mathcal{P} \equiv n\text{Tr}[\rho\mathbf{d}_\downarrow] \equiv n\mathbf{p}, \quad (\text{S5})$$

where n is the local atomic number density and \mathbf{d}_\downarrow is the dipole operator describing downward transitions. For the atom distribution, we take a Gaussian with FWHM $2\sigma_T\sqrt{\ln 2}$ and $2\sigma_L\sqrt{\ln 2}$ in the transverse and longitudinal directions, respectively:

$$n(\mathbf{x}) = N_A(\pi^{3/2}\sigma_L\sigma_T^2)^{-1} \exp[-r^2/\sigma_T^2] \exp[-z^2/\sigma_L^2] \quad (\text{S6})$$

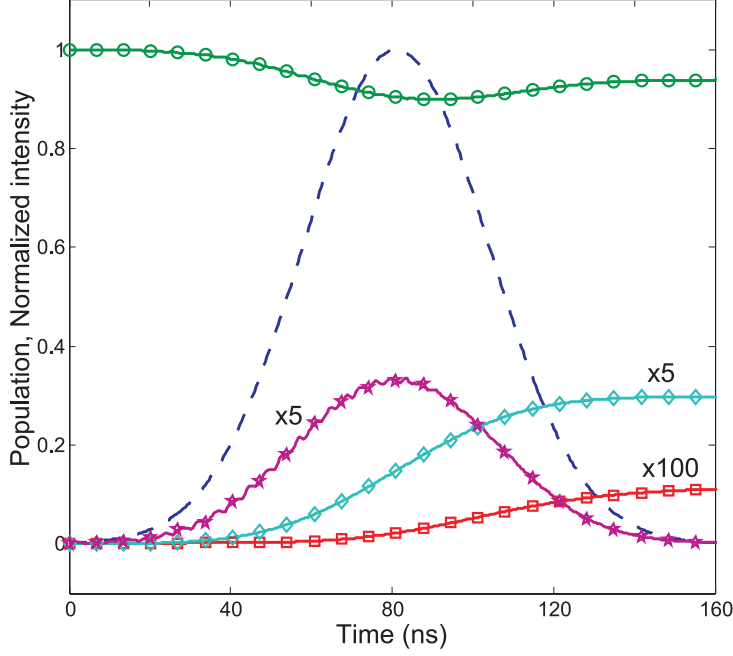
where $r^2 \equiv x^2 + y^2$.

We solve to first order in N_A as follows. We identify a solution to the zero-atom equation $\mathcal{D}\mathcal{E} = 0$ as the input field $\mathcal{E}^{(\text{in})}$. Specifically, we take $\mathcal{E}^{(\text{in})} = \mathcal{E}_0\mathbf{e}_V T(\tau)M(\mathbf{x})$ where \mathbf{e}_V is the unit vector in the V direction,

$$T(\tau) = \pi^{-1/4}\tau^{-1/2} \exp[-t^2/2\tau^2] \quad (\text{S7})$$

is a Gaussian pulse with FWHM $2\tau\sqrt{\ln 2}$, and

$$M(\mathbf{x}) = \sqrt{\frac{2}{\pi w^2(z)}} \exp[-r^2/w^2(z)] \exp[i\psi(r, z)] \quad (\text{S8})$$



Supp. Fig. 4: Population dynamics under nonlinear probing. Results of simulations for a Gaussian pulse with a FWHM of 54ns, 5.7 million photons, a peak intensity of 4W/cm² and $\Delta = 462$ MHz, with an initially-polarized density matrix. Blue dashed line, pulse intensity (normalized). Symbols show total population for groups of states: Green circles, $|1, 1\rangle$ state; red squares, $|1, -1\rangle$ and $|1, 0\rangle$ states ($100 \times$ magnified); purple stars, excited states ($5 \times$ magnified); turquoise diamonds, $F = 2$ states ($5 \times$ magnified).

where $w^2(z) = w_0^2(1 + z^2/z_R^2)$, $z_R = \pi w_0^2/\lambda$, and ψ is the wave-front phase. This describes a Gaussian beam with effective area $A_0 \equiv \int dx dy |M(x, y, 0)|^2 / |M(\mathbf{0})|^2 = \pi w_0^2/2$.

We find numerically the solution to Eq. (S4) with $\mathcal{E} = \mathcal{E}^{(\text{in})}$ as the lowest-order atomic response $\rho^{(1)}$. A representative case is shown in Supp. Fig. 4. The evolving atomic state generates the field

$$\mathcal{E}^{(1)}(\mathbf{x}, \tau) = \frac{k^2}{\varepsilon_0} \int d^3x' G(\mathbf{x}, \mathbf{x}') \mathcal{P}^{(1)}(\mathbf{x}', \tau) \quad (\text{S9})$$

where G is the Green function for the PWE.

The detected signal is $\langle \hat{S}_y \rangle \equiv (\hbar\omega Z_0)^{-1} \int d^2x d\tau \mathcal{E}_V^{(\text{in})*} \mathcal{E}_H^{(1)} + c.c.$, where the spatial integral is taken over the surface of the detector and subscripts H, V indicate polarization components. It

can be shown, e.g., using Green function techniques²⁶, that

$$\int d^2x d\tau \mathcal{E}_V^{(\text{in})*} \mathcal{E}_H^{(1)} = \frac{k}{2i\varepsilon_0} \int d^3x d\tau \mathcal{E}_V^{(\text{in})*} \mathcal{P}_H^{(1)} \quad (\text{S10})$$

and thus

$$\langle \hat{S}_y \rangle = (\hbar\omega Z_0)^{-1} \frac{k}{2i\varepsilon_0} \int d^3x n \int d\tau \mathcal{E}_V^{(\text{in})*} p_H^{(1)} + c.c. \quad (\text{S11})$$

while $\langle \hat{S}_x \rangle = (\hbar\omega Z_0)^{-1} \int d^2x d\tau |\mathcal{E}_V^{(\text{in})}|^2 = (\hbar\omega Z_0)^{-1} |\mathcal{E}_0|^2$.

Independently determined values for the model parameters σ_L, σ_T, w_0 and τ are used, leaving only N_A as a free parameter, found by fitting to the data. We note that N_A determines the vertical position of the curve in Figure 3, and has no effect on the sensitivity scaling. In this sense, the model confirms the scaling behaviour with no adjustable parameters.

Simulations indicate that loss of polarization in $F = 1$, and thus rotation signal, is mostly due to spontaneous decay into the $F=2$ ground level, as seen in Supp. Fig. 4.

Sensitivity in time- and number-limited scenarios When time is limiting, the relevant sensitivity is $\delta F_z \tau^{1/2}$, where $\delta F_z = \langle \hat{F}_z \rangle \delta\phi/\phi$ as in Equation 1, and the measurement duration τ is $\tau_L = 40 \mu\text{s}$ or $\tau_{\text{NL}} = 54 \text{ ns}$ for the linear or nonlinear measurement, respectively. The sensitivity can be calculated from the measured values $A(\Delta_L) = 3.3 \times 10^{-8}$, and $B(\Delta_0) = 3.8 \times 10^{-16}$, using $\delta\phi = N^{-1/2}/2$, $\phi_L/\langle \hat{F}_z \rangle = A(\Delta_L)/2$ and $\phi_{\text{NL}}/\langle \hat{F}_z \rangle = B(\Delta_0)N_{\text{NL}}/2$. We find $\delta F_z^{(\text{L})} \tau_L^{1/2} = 1.9 \times 10^5 \text{ Hz}^{-1/2} N_L^{-1/2}$, and $\delta F_z^{(\text{NL})} \tau_{\text{NL}}^{1/2} = 6.1 \times 10^{11} \text{ Hz}^{-1/2} N_{\text{NL}}^{-3/2}$. Given an equal number of photons $N_L = N_{\text{NL}} = N$, the nonlinear technique surpasses the linear at $N = 3.2 \times 10^6$, well within the super-Heisenberg portion of the curve in Figure 3. In contrast, when time is not a

limited resource, the sensitivity-per-measurement is $\delta F_z^{(L)} = 3 \times 10^7 N_L^{-1/2}$, and $\delta F_z^{(NL)} = 2.6 \times 10^{15} N_{NL}^{-3/2}$. Extrapolating, the nonlinear technique would surpass the linear at $N_{NL} = 8.7 \times 10^7$, which is however outside the super-Heisenberg portion of the curve in Figure 3.

Supplementary Notes

25. Windpassinger, P. J. *et al.* Ultra low-noise differential ac-coupled photodetector for sensitive pulse detection application. *Meas. Sci. Technol.* **20**, 0055201 (2009)
26. Mitchell, M. W. Parametric down-conversion from a wave-equation approach: Geometry and absolute brightness. *Phys. Rev. A* **79**, 043835 (2009)